ChemComm

COMMUNICATION

View Article Online
View Journal

Cite this: DOI: 10.1039/d6cc01364c

Received 6th March 2026,
Accepted 15th April 2026

DOI: 10.1039/d6cc01364c

rsc.li/chemcomm

Continuous-flow electrochemical production of H_2O_2 in a gas diffusion electrode microreactor

Desislava Yordanova Apostolova,[a] Ema Gričar,[a] Maris Minna Mathew,[a] Tomaž Gril,[a] Miha Nosan,[a] Ivo Bardarov[ab] and Boštjan Genorio *[a]

A microfluidic electrochemical reactor equipped with a gas diffusion cathode continuously produced up to 22.3 mM H_2O_2, with ~88% faradaic efficiency and an energy consumption of 5.1 kWh kg^{-1}. This performance surpasses current membraneless electrochemical H_2O_2 production processes, eliminating the need for a membrane or separator while maintaining high efficiency.

Decentralized electrochemical production of hydrogen peroxide (H_2O_2) offers a sustainable, energy-efficient and green alternative to the anthraquinone process. However, the decentralized process is still limited by the oxygen mass transport and reactor design limitations. Here, we report a modified microfluidic electrochemical reactor that integrates a gas diffusion electrode (GDE) cathodic half-cell to mitigate oxygen transport limitations in the selective two-electron oxygen reduction reaction (2e$^-$ ORR). Direct comparison against a parallel-plate configuration[1] reveals significantly enhanced H_2O_2 productivity and oxygen utilization. Coupled with in-line optical monitoring of H_2O_2 production and additional testing with an off-line electrochemical sensor, this work clarifies the decisive role of microreactor architecture in governing H_2O_2 selectivity in a metal-free system.

H_2O_2 is an environmentally benign oxidant widely used in bleaching, wastewater treatment, chemical synthesis, and energy storage/conversion,[2–4] with steadily increasing global demand.[5] Industrial production is dominated by the centralized anthraquinone process, which requires hydrogen, organic solvents, and platinum group metals (PGMs), and involves transportation of concentrated H_2O_2, posing safety and logistical challenges.[6] Electrochemical synthesis offers a decentralized and potentially safer route *via* a two-electron oxygen reduction reaction in alkaline media (eqn (1)).

$$O_2 + H_2O + 2e^- \rightarrow HO_2^- + OH^- \quad E^0 = 0.74\ \text{V vs. RHE} \quad (1)$$

In alkaline solution, hydroperoxide (HO_2^-) is formed (pK_a of H_2O_2 = 11.6); however, sluggish kinetics and limited oxygen solubility in aqueous electrolytes constrain overall efficiency.[7,8] Although PGMs and their alloys achieve selectivity up to 98%,[9–11] their cost and scarcity restrict scalability. Carbon-based electrodes have therefore emerged as promising low-cost alternatives.[12–14]

Beyond electrocatalyst composition, reactor design critically governs oxygen delivery and H_2O_2 production. Ion-exchange membrane systems and GDE-based electrolyzers improve oxygen utilization and product concentration.[15–17] On the other hand, membraneless microfluidic electrochemical flow cells enhance mass transport by controlling flow rate and optimizing channel dimensions, while also helping to minimize reactant crossover.[18,19] Nevertheless, systematic comparisons of different reactor architectures and their direct impact on H_2O_2 production remain limited. In addition, quantification is typically performed *ex situ* rather than through *in situ* measurements.[20–22]

By integrating a GDE cathodic half-cell into a microfluidic platform and comparing it against a parallel-plate microreactor, we demonstrate how gaseous oxygen supply directly governs H_2O_2 production and selectivity. The optimized, metal-free configuration establishes practical design principles for efficient, decentralized electrochemical H_2O_2 synthesis.[1,23]

The electrochemical microreactor housing was fabricated by CNC milling from PTFE blocks (Fig. 1(a)). The microreactor has an internal channel volume of 21.6 μL, corresponding to a retention time of 25.9 s at a flow rate of 50 μL min^{-1} (eqn (S1)). In the anode compartment, a glassy carbon (GC) electrode was embedded and served as the counter electrode. The cathode compartment was equipped with a gas inlet and an integrated gas flow channel to accommodate the gas diffusion electrode (GDE). The gas diffusion layer (GDL) consisted of carbon paper (Sigracet 22 BB, Fuel Cell Store). The catalyst ink, prepared using Ketjenblack EC-300J (KJB EC-300J), ultrapure water (resistivity of 18.2 MΩ cm), 2-propanol (IPA), and Nafion 117 solution, was deposited onto the GDL by spray-coating. Multiple GDEs were prepared with a target electrocatalyst loading of 300 μg cm^{-2} on a GDL working electrode (WE) with an area of

[a] *Faculty of Chemistry and Chemical Technology, University of Ljubljana, Večna pot 113, 1000 Ljubljana, Slovenia. E-mail: bostjan.genorio@fkkt.uni-lj.si*
[b] *Department of Chemistry, South-West University "Neofit Rilski", 66 Ivan Mihajlov Str., 2700 Blagoevgrad, Bulgaria*

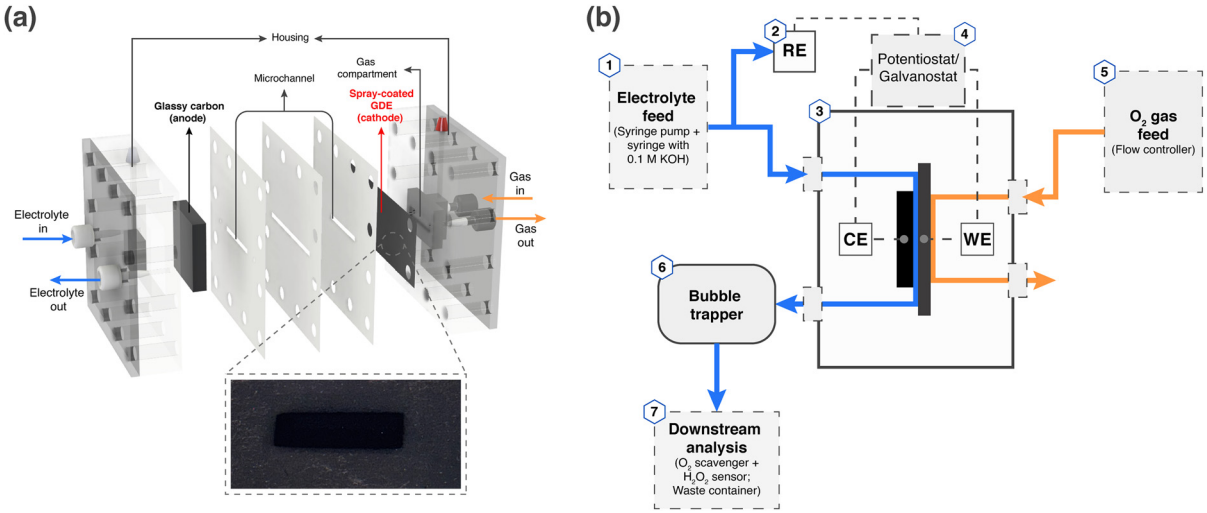

Fig. 1 (a) Schematic of the microfluidic electrochemical reactor configured as a GDE half-cell; inset: the GDL with the spray-coated electrocatalyst. (b) Flow diagram of the experimental setup, including gas and electrolyte supply, reactor assembly, and product analysis.

36 mm^2 (inset of Fig. 1(a)). Full details of the ink formulation and the preparation procedure are provided in the SI. A reference electrode (Ag/AgCl/3 M NaCl, BASi Research) was placed in a separate sealed vial connected to the microchannel system that supplied electrolyte to the reactor (Fig. 1(b)). All potentials are reported *versus* the reversible hydrogen electrode (RHE). The electrolyte (O_2-saturated 0.1 M KOH) was delivered through the microreactor using a syringe pump. H_2O_2 production was monitored using an in-line optical detection system,[21] and, for high current chronopotentiometric (CP) measurements, an off-line electrochemical sensor[20] was used.

Electrochemical measurements were performed using a potentiostat/galvanostat (BioLogic SP-300). Full details of the electrochemical measurements and data acquisition are provided in the SI.

Before and after electrosynthesis experiments, characterization of the GDE electrodes was performed using scanning electron microscopy (SEM) coupled with energy-dispersive X-ray spectroscopy (EDS), Raman spectroscopy and X-ray photoelectron spectroscopy (XPS) (Fig. S3–S6). Cross-sectional SEM images (Fig. 2(a) and (b)) show that the spray-coated catalyst ink is deposited on the microporous layer (MPL), while the backing (support) layer of the GDE is clearly visible beneath it (shown in Fig. S3). Compared with the freshly coated sample, SEM analysis indicates no visible morphological changes; however, EDS analysis reveals an increased oxygen content on the catalyst surface after the electrochemical experiments.

This suggests surface oxidation during electrosynthesis of H_2O_2, which was further confirmed by the XPS results presented in Table 1.

The system (Fig. 1(b)) was designed to enable controlled CP for continuous-flow electrochemical H_2O_2 production in 0.1 M KOH and O_2 flow to the cathode half-cell, while allowing real-time monitoring of H_2O_2 concentration using an integrated in-line optical sensor. Electrolyte flow was maintained at 50 μL min^{-1} using a syringe pump directly connected to the microreactor, and a mass flow controller regulated the O_2 supply. The reference electrode was in electrolytic contact with the microreactor. Immediately downstream of the microreactor, an in-line bubble remover was installed to eliminate bubbles generated during the electrochemical measurements, likely originating from oxygen

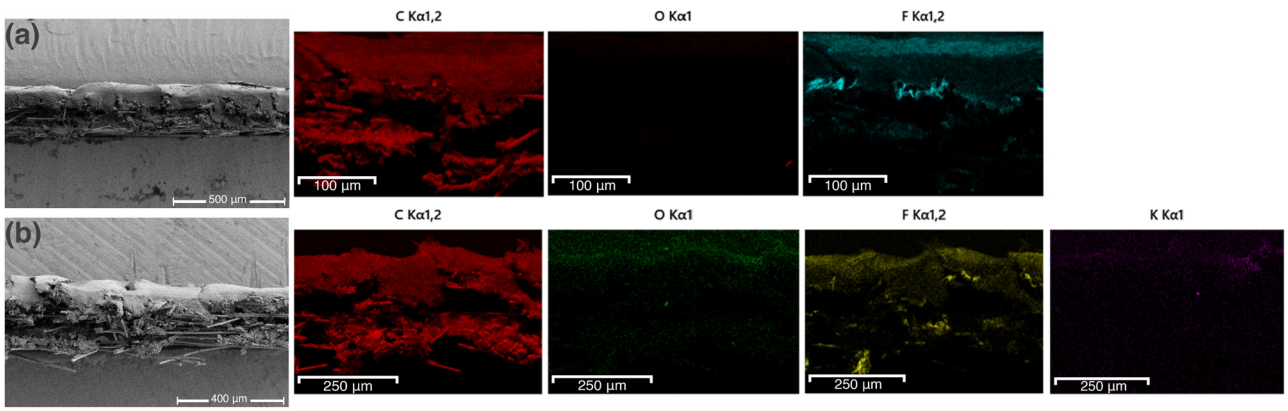

Fig. 2 SEM images and the corresponding EDS analysis of the KJB EC-300J spray-coated GDE: (a) before and (b) after electrochemical measurements. The upper part corresponds to the catalyst layer on the microporous GDL.

Table 1 Oxygen content (EDS/XPS) of KJB EC300-J coated GDEs (WE) before and after electrochemistry

	EDS [wt%] before EC	EDS [wt%] after EC	XPS [at%] before EC	XPS [at%] after EC
WE	1.7	4.1	5.26	9.56

evolution at the counter electrode.[1] This ensured uninterrupted flow to the optical sensor during H_2O_2 monitoring.

At the core of the system is the microreactor equipped with a GDE half-cell. KJB EC-300J powder was selected as the electrocatalyst due to its high selectivity and excellent processability, enabling the preparation of homogeneous catalyst inks. Before integration into the microfluidic setup, the electrocatalyst was evaluated using the rotating ring-disk electrode (RRDE) technique to determine H_2O_2 selectivity, which was found to be above 80% in the potential range 0.4–0.6 V *vs.* RHE (Fig. S7), a key requirement for this study.

Electrochemical impedance spectroscopy (EIS) measurements were performed before all electrochemical experiments, confirming an electrolyte resistance of 2–3 Ω for all measurements. The CP measurements were performed on different GDEs with similar loadings, using currents determined from cyclic voltammetry (CV), with current values selected based on specific potentials. As shown in Fig. S8, obtaining fully reproducible CVs at this stage was challenging. Nevertheless, the KJB EC-300J H_2O_2 selectivity at specific potentials on the GDE agrees with RRDE measurements.

Recorded potentials of the WE during CP are shown in Fig. 3(a), with the corresponding H_2O_2 concentrations shown in Fig. 3(b). As expected, the measured H_2O_2 concentration increased with increasing applied current, reaching an average maximum of 22.3 mM at $i = -4.11$ mA (currents taken from CVs at $E = 0.4$ V *vs.* RHE). This represents approximately a 50-fold increase in H_2O_2 production compared with our previously published parallel-plate microreactor system,[1] indicating that the implementation of a GDE and improved control over oxygen mass transport significantly enhance H_2O_2 production.

One limitation of applying high currents is the reduced reliable detection range of the in-line optical sensor. Up to reductive currents of 1.5 mA, the optical sensor functioned reliably, providing linear H_2O_2 determination shown in Fig. S2(a) and (b) with a correlation coefficient of 0.991. The H_2O_2 concentrations obtained from the in-line detection system are calculated using eqn (S2). However, at reductive currents exceeding 2 mA, reliable measurements were no longer possible due to the detection limit of the optical sensor. For these high-current measurements, an off-line electrochemical sensor was employed to determine reliable H_2O_2 concentrations. The calibration of the off-line electrochemical sensor is presented in Fig. S2(c). Detailed H_2O_2 concentrations from in-line and off-line detection are presented in Table S1.

The application of high currents also suggested possible electrocatalyst deactivation, as evidenced by the increased variability of the recorded WE potential. As shown in Fig. S9, WE and counter electrode (CE) potentials were stable at currents up to $i = -2.4$ mA, but at higher currents (Fig. S9(f)–(i)), the WE potential gradually dropped over time, indicating the need for higher overpotential to maintain H_2O_2 production. An exception was observed in Fig. S9(h), where, following a substantial potential drop, the measurement stabilized for the remainder of the experiment. We hypothesize that this behaviour may reflect *in situ* activation of the catalyst during electrochemical operation.

To investigate this possibility, consecutive CPs at various currents were performed on the same electrode (Fig. S10). The results indicate that a potential drop occurs at $i = -1.5$ mA, and subsequent repetitions suggest possible catalyst activation, as the system became more stable. While these observations are consistent with *in situ* activation (as indicated by the increase of oxygen content in Table 1), the exact mechanism remains unclear, and further studies are underway to confirm this phenomenon.

Faradaic efficiency (FE) was calculated using eqn (S3) for all electrochemical measurements. As shown in Fig. 3(c), the FE remained high, ranging from 63.2% to 87.5%, with the maximum observed at the highest H_2O_2 concentration. These results demonstrate the high efficiency of the system for the two-electron oxygen reduction reaction to H_2O_2.

The specific energy consumption of the system was calculated using eqn (S5) for the measurements that produced the highest H_2O_2 concentration based on the experimentally determined full-cell potential (eqn (S4) and Table S2). This resulted in an energy cost of approximately 5.12 kWh kg^{-1} H_2O_2, representing the average of four independent measurements performed under the best-performing operating conditions. For comparison,

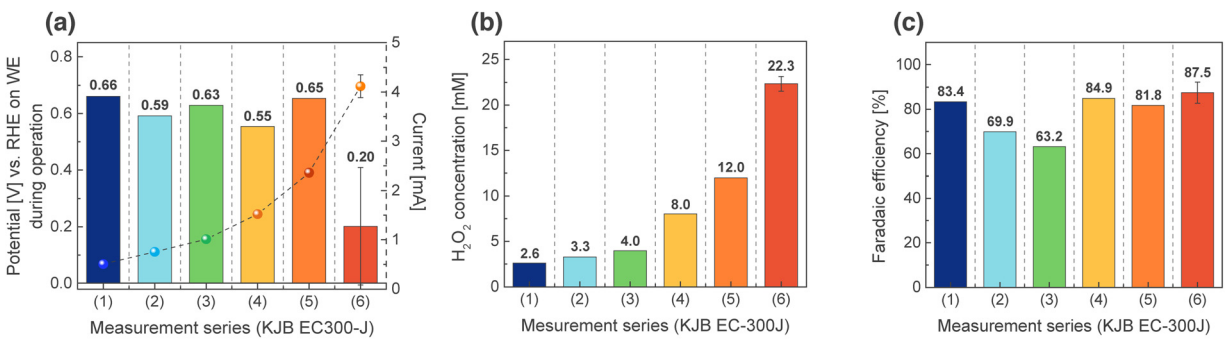

Fig. 3 (a) Potentials recorded during CP measurements (bar graph) with the corresponding applied reductive currents (spheres). (b) H_2O_2 concentration over the course of reactor operation. (c) Corresponding faradaic efficiency.

state-of-the-art electrochemical systems using a gas diffusion electrode with a membrane assembly consume 6.67 kWh kg^{-1} H_2O_2,[24] indicating that the current membraneless configuration reduces energy consumption by about 23%. Although the conventional anthraquinone process requires 2.5–3.5 kWh kg^{-1} H_2O_2,[25] these results show that the present system achieves competitive energy efficiency, even at this preliminary stage. The variation in energy efficiency observed between different measurement series (Table S2) can be attributed to minor fluctuations in cell voltage and H_2O_2 production, resulting from differences in oxygen mass transport, electrode wetting, and experimental uncertainties in product quantification.

In summary, a microfluidic electrochemical system with a gas diffusion electrode (GDE) enables efficient and controlled H_2O_2 production under alkaline conditions. Post-operation characterization showed increased surface oxygen content, indicating surface oxidation during catalysis that may contribute to catalyst activation. Real-time H_2O_2 monitoring with an in-line optical sensor, combined with continuous electrolyte flow and bubble management, ensures stable operation. H_2O_2 concentration increased with applied current, reaching 22.3 mM – approximately 50 times higher than a previously reported parallel-plate microreactor. High faradaic efficiencies (~63–88%) confirm the dominance of the two-electron oxygen reduction reaction. Although optical sensor limitations and gradual catalyst deactivation occur at high currents, off-line measurements validate H_2O_2 profiles. The system achieves competitive energy consumption (~5.12 kWh kg^{-1} H_2O_2), approaching the efficiency of the anthraquinone process and highlighting the potential of GDE-based membraneless microfluidic platforms for selective H_2O_2 electrosynthesis.

Author contributions

Desislava Yordanova Apostolova: writing – review & editing, writing – original draft, visualization, investigation, formal analysis, conceptualization. Ema Gričar: writing – review & editing, investigation, formal analysis. Maris Minna Mathew: writing – review & editing, investigation. Tomaž Gril: investigation, visualization. Miha Nosan: writing – review & editing, conceptualization. Ivo Bardarov: conceptualization. Boštjan Genorio: writing – review & editing, writing – original draft, visualization, supervision, project administration, methodology, investigation, funding acquisition, formal analysis, conceptualization.

Conflicts of interest

The authors declare that they have no known competing financial interests or personal relationships that could have appeared to influence the work reported in this paper.

Data availability

The data supporting this article have been included as part of the supplementary information (SI). The Supplementary information includes experimental protocols, characterization data, and extended experimental results, and is available at DOI: https://doi.org/10.1039/d6cc01364c.

Raw data that support the findings of this study are available from the corresponding author upon reasonable request.

Acknowledgements

The financial support from the Slovenian Research and Innovation Agency (ARIS) through grants P2-0423, P1-0447, J7-4636, J2-50086, J7-50227, J2-60044, and L2-3161 and the infrastructure program I0-0022 is gratefully acknowledged. The authors would like to thank Torsten Mayr and Anders Ø. Tjell from TU Graz for providing the in-line optical H_2O_2 sensors. D. Y. Apostolova warmly thanks Jan Táborský for his assistance with the spray-coating procedure.

References

1 D. Y. Apostolova, I. Bardarov, A. Tjell, E. Gričar, M. Starin, P. F. B. D. Martins, M. Nosan, T. Mayr, D. Strmčnik, I. Plazl and B. Genorio, A parallel-plate electrochemical microreactor for the continuous production of hydrogen peroxide, *Chem. Eng. J.*, 2025, **525**, 170301.
2 S. C. Perry, D. Pangotra, L. Vieira, L. I. Csepei, V. Sieber, L. Wang, C. Ponce de León and F. C. Walsh, Electrochemical synthesis of hydrogen peroxide from water and oxygen, *Nat. Rev. Chem.*, 2019, **3**, 442–458.
3 R. Hage and A. Lienke, Applications of transition-metal catalysts to textile and wood-pulp bleaching, *Angew. Chem., Int. Ed.*, 2005, **45**, 206–222.
4 S. Chen, Z. Chen, S. Siahrostami, T. R. Kim, D. Nordlund, D. Sokaras, S. Nowak, J. W. F. To, D. Higgins, R. Sinclair, J. K. Nørskov, T. F. Jaramillo and Z. Bao, Defective Carbon-Based Materials for the Electrochemical Synthesis of Hydrogen Peroxide, *ACS Sustainable Chem. Eng.*, 2018, **6**, 311–317.
5 Hydrogen Peroxide Market Size, Share|Growth Report, 2034, https://www.fortunebusinessinsights.com/hydrogen-peroxide-market-103920, accessed 24 February 2026.
6 J. M. Campos-Martin, G. Blanco-Brieva and J. L. G. Fierro, Hydrogen peroxide synthesis: An outlook beyond the anthraquinone process, *Angew. Chem., Int. Ed.*, 2006, **45**, 6962–6984.
7 A. Verdaguer-Casadevall, D. Deiana, M. Karamad, S. Siahrostami, P. Malacrida, T. W. Hansen, J. Rossmeisl, I. Chorkendorff and I. E. L. Stephens, Trends in the electrochemical synthesis of H_2O_2: Enhancing activity and selectivity by electrocatalytic site engineering, *Nano Lett.*, 2014, **14**, 1603–1608.
8 X. Zhao and Y. Liu, Origin of Selective Production of Hydrogen Peroxide by Electrochemical Oxygen Reduction, *J. Am. Chem. Soc.*, 2021, **143**, 9423–9428.
9 Z. Lu, G. Chen, S. Siahrostami, Z. Chen, K. Liu, J. Xie, L. Liao, T. Wu, D. Lin, Y. Liu, T. F. Jaramillo, J. K. Nørskov and Y. Cui, High-efficiency oxygen reduction to hydrogen peroxide catalysed by oxidized carbon materials, *Nat. Catal.*, 2018, **1**, 156–162.
10 Z. Zheng, Y. H. Ng, D. W. Wang and R. Amal, Epitaxial Growth of Au–Pt–Ni Nanorods for Direct High Selectivity H_2O_2 Production, *Adv. Mater.*, 2016, **28**, 9949–9955.
11 H. Yang, W. Vogel, C. Lamy and N. Alonso-Vante, Structure and Electrocatalytic Activity of Carbon-Supported Pt-Ni Alloy Nanoparticles Toward the Oxygen Reduction Reaction, *J. Phys. Chem. B*, 2004, **108**, 11024–11034.
12 M. Nosan, D. Strmčnik, V. Brusko, M. Kirsanova, M. Finšgar, A. M. Dimiev and B. Genorio, Correlating nickel functionalities to selectivity for hydrogen peroxide electrosynthesis, *Sustainable Energy Fuels*, 2023, **7**, 2270–2278.
13 I. Bardarov, D. Y. Apostolova, M. M. Mathew, M. Nosan, P. F. B. Dias Martins and B. Genorio, Flash Graphene: a Sustainable Prospect for Electrocatalysis, *Acta Chim. Slov.*, 2024, **71**, 541–557.
14 C. X. Zhao, B. Q. Li and Q. Zhang, Advanced electrosynthesis of hydrogen peroxide on oxidized carbon electrocatalyst, *J. Energy Chem.*, 2019, **34**, 10–11.

15 X. Zhang, Y. Xia, C. Xia and H. Wang, Insights into Practical-Scale Electrochemical H_2O_2 Synthesis, *Trends Chem.*, 2020, **2**, 942–953.
16 C. Xia, Y. Xia, P. Zhu, L. Fan and H. Wang, Direct electrosynthesis of pure aqueous H_2O_2 solutions up to 20% by weight using a solid electrolyte, *Science*, 2019, **366**, 226–231.
17 Z. Chen, S. Chen, S. Siahrostami, P. Chakthranont, C. Hahn, D. Nordlund, S. Dimosthenis, J. K. Nørskov, Z. Bao and T. F. Jaramillo, Development of a reactor with carbon catalysts for modular-scale, low-cost electrochemical generation of H_2O_2, *React. Chem. Eng.*, 2017, **2**, 239–245.
18 P. Farinazzo Bergamo Dias Martins, I. Plazl, D. Strmcnik and B. Genorio, Prospect of microfluidic devices for on-site electrochemical production of hydrogen peroxide, *Curr. Opin. Electrochem.*, 2023, **38**, 101223.
19 R. Ferrigno, A. D. Stroock, T. D. Clark, M. Mayer and G. M. Whitesides, Membraneless vanadium redox fuel cell using laminar flow, *J. Am. Chem. Soc.*, 2002, **124**, 12930–12931.
20 E. Gričar, K. Kalcher, B. Genorio and M. Kolar, Highly sensitive amperometric detection of hydrogen peroxide in saliva based on n-doped graphene nanoribbons and MnO_2 modified carbon paste electrodes, *Sensors*, 2021, **21**, 8301.
21 A. Tjell, B. Jud, R. Schaller-Ammann and T. Mayr, Optical hydrogen peroxide sensor for measurements in flow, *Sens. Actuators, B*, 2024, **400**, 134904.
22 V. Lvovich and A. Scheeline, Amperometric Sensors for Simultaneous Superoxide and Hydrogen Peroxide Detection, *J. Electroanal. Chem.*, 1987, **69**, 454–462.
23 W. Xing, H. China and J. Zhang, *Rotating electrode methods and oxygen reduction electrocatalysts*, National Research Council of Canada, 2014.
24 Y. Zhao, N. Deng, Z. Fan, Z. T. Hu, L. Fan, J. Zhou and X. Huang, On-site H_2O_2 electro-generation process combined with ultraviolet: A promising approach for odorous compounds purification in drinking water system, *Chem. Eng. J.*, 2022, **430**, 132829.
25 P. Westbroek and E. Temmerman, Mechanism of hydrogen peroxide oxidation reaction at a glassy carbon electrode in alkaline solution, *J. Electroanal. Chem.*, 2000, **482**, 40–47.